COUPLING-CURRENT AND PERSISTENT-CURRENT MAGNETIZATIONS IN Nb_3Sn RUTHERFORD CABLES AND STRANDS

E.W. Collings[1] , M.D. Sumption[1], M.A. Susner[1], D.R. Dietderich[2], E. Barzi[3], A.V. Zlobin[3], and A. Nijhuis[4]

[1]Center for Superconducting and Magnetic Materials (CSMM), MSE Dept., The Ohio State University, Columbus, OH 43210, USA

[2] Superconducting Magnet Group, Lawrence Berkeley National Laboratory (LBNL), Berkeley, CA 94720, USA

[3] Fermi National Accelerator Laboratory (FNAL), Batavia, IL 60510, USA

[4] Low Temperature Division, Faculty of Applied Physics, University of Twente, Enschede, NL

ABSTRACT

Calorimetric and magnetic measurements of AC loss in Nb_3Sn Rutherford cables were accompanied by magnetic measurements of persistent-current (hysteretic) loss in strands extracted from those cables. From the cable-loss measurements it is shown that the introduction of a stainless steel core increases the effective interstrand contact resistance (ICR), initially 0.3 μΩ, by more than two orders of magnitude. Uniaxial pressure applied to the cable during winding and subsequently, seemingly by reducing side-by-side contact, increased the ICR. In an edge-on applied AC field the persistent-current cable loss was fully accounted for in terms of the individual-strand loss. The persistent-current loss measured for the cable in a face-on applied field was higher that that in an edge-on applied field, this may have been due to demagnetization effects.

KEYWORDS: Nb_3Sn, Rutherford cable, strand, coupling current, interstrand contact resistance, uniaxial pressure, persistent current, magnetization

CP1219, *Advances in Cryogenic Engineering: Transactions of the Cryogenic Engineering Materials Conference - ICMC, Vol. 56,* edited by U. Balachandran

INTRODUCTION

Multistrand Rutherford cables are the conductor of choice for particle beam steering and focusing magnets for high energy physics applications. These cables may exhibit two classes of parasitic magnetization either of which can distort the field of the host magnet. They are: (1) A *static magnetization* ("hysteretic") resulting from the intrastrand ***persistent*** currents. (2) A *dynamic magnetization* that is produced by interstrand ***coupling*** currents generated by time-varying magnet excitation. Both persistent currents and coupling currents produce cable magnetization components that distort the bore fields of accelerator dipoles and quadrupoles [1]. In order to achieve tight control of the particle beam during injection, acceleration, and storage it is necessary to minimize these field distortions. Coupling control is achieved by ensuring that for accelerator cables in general (e.g. [2]) the strand-cross-over-contact resistance (ICR), denoted $R_{\perp}$, is in the vicinity of 20 ± 10 μΩ [2] and that the side-by-side resistance, $R_{//}$, although relatively small, is not less than 0.2 μΩ [3]. Over the years numerous techniques have been employed to suppress parasitic magnetization and improve field quality especially in accelerator dipole and quadrupole magnets. Looking ahead to the use of Nb_3Sn for the LHC's anticipated luminosity upgrades [4] the parasitic magnetization issues are being revisited. Both coupling- and persistent-current magnetizations are stronger in Nb_3Sn cables.

Coupling Magnetization

The coupling-generated field errors that were encountered in dipoles and quadrupoles made with NbTi-based cables will again appear in their Nb_3Sn counterparts unless suitable precautions are taken. Under Large Hadron Collider (LHC) operating conditions, field errors will be acceptably low provided the cables meet the above-quoted $R_{\perp}$ and $R_{//}$ specifications. In cable characterization studies these resistances can be measured ohmically [2][5]. They can also be extracted from the results of AC-loss measurements purposely carried out, as described below and elsewhere [6] at relatively high applied-field ramp-rates or frequencies. As explained in [7] the coupling loss per cycle per m^3 of a cable (width, w, thickness, t, strand count, N, transposition pitch, $2L_p$) exposed to fields linearly ramping at a rate dB/dt to amplitude B_m applied perpendicular (face-on, FO, leading to $Q_{\perp}$) to the cable's broad face is given by:

$$Q_{\perp} = \left(\frac{4}{3}\right)\left(\frac{w}{t}\right) L_p B_m \left[\frac{N^2}{20R_{\perp}} + \frac{1}{NR_{//}}\right].\left(\frac{dB}{dt}\right) \qquad (1)$$

When calculating the expected coupling loss in a Rutherford cable exposed to a relatively low frequency, sinusoidal, oscillating applied field, it is useful to note that the ramp-rate can be transformed to frequency using $dB/dt = (\pi^2/2)B_m f$ [7], after which Equation (1) becomes

$$Q_{\perp}(f) = \left(\frac{\pi^2}{30}\right)\left(\frac{w}{t}\right) L_p B_m^2 N^2 \left[\frac{1}{R_{\perp}} + \frac{20}{N^3 R_{//}}\right].f \qquad (2)$$

Equation (2) expresses the FO loss in the ICR network in terms of a pair of parallel resistors $R_{\perp}$ and $(N^3/20)R_{//}$ enabling an $R_{\perp,eff}$ defined as $1/R_{\perp,eff} = 1/R_{\perp} + 20/N^3 R_{//}$ to be extracted from the reciprocal initial slope of $Q_{\perp}$ vs f. Picture a 28-strand cable with

"standard" ICRs of 20 μΩ ($R_\perp$) and 0.2 μΩ ($R_{//}$). The parallel-resistor model would then consist of an $R_\perp$ (with value 20 μΩ) bypassed by 200 μΩ. Thus to a first approximation the $R_{\perp,eff}$ of a simple Rutherford cable can be regarded as the crossover resistance $R_\perp$. Clearly $R_{\perp,eff}$ can be increased either by coating the strands (with simultaneous increases in $R_\perp$ and $R_{//}$) or by introducing a core (which increases just $R_\perp$). For a cored cable $R_{\perp,eff} = (N^3/20)R_{//}$.

As a property of the cable rather than the strand the coupling loss or magnetization is independent on whether the cable is wound with NbTi or Nb_3Sn. Hence for both classes of cable the coupling magnetization in a face-on field is

$$M_{coup} = \frac{Q_\perp}{4B_m} = \frac{1}{3}\left(\frac{w}{t}\right)L_p\left(\frac{dB}{dt}\right)\frac{N^2}{20R_{\perp,eff}} \tag{3}$$

In LHC operation, following proton injection at 0.54 T (450 GeV) the field is ramped to 8.36 T (7 TeV) in about 1000 s hence at a ramp rate dB/dt of 6.5 mT/s. The coupling magnetization of the LHC-inner cable, for example, can then be deduced by substituting $(w/t) = 15/1.89 = 7.94$, $L_p = 55$ mm and $N = 28$, after which $M_{coup} = 37.1/R_{\perp,eff(\mu\Omega)}$ kA/m. At a recommended $R_{\perp,eff}$ of say 20 μΩ, we obtain an M_{coup} during the ramp of 1.9 kA/m, a value which is much less than that produced by persistent current.

Persistent-Current Magnetization

It is generally recognized that the most important contributor to field error at injection is the persistent-current ("hysteretic") magnetization of the superconducting strand [8]. This materials-dependent magnetization, already present during the early stage of injection, is given by $M_h = (2/3\pi)\lambda J_c d$ in which λ is the superconducting fill factor and d is the filament diameter. The magnetization M_h can be calculated from the strand properties or obtained by direct measurement, as in the case of LHC for which strand magnetization was an acceptance specification. For a Technical Quadrupole (TQ)-class strand at 1.9 K the magnetizations at 5 T and 12 T are estimated to be 94 kA/m and 25 kA/m, respectively.

EXPERIMENTAL

Materials, Sample Preparation, and Measuring Techniques

Three lengths of TQ-class 27-strand Rutherford cable were provided by the Lawrence Berkeley National Laboratory (LBNL). Two of them were furnished with a core of 316L stainless steel strip, 8 mm wide and 25 μm thick, TABLE 1. After the initial pass through the machine, the cables were annealed for 4h/200°C and two of them re-rolled. Segments of these cables, each 20 inches long, were wrapped with s-glass tape (about 25% overlap) in readiness for assembly into three cable packs. As described elsewhere [9] on the way to being vacuum impregnated and trimmed to length the cable packs received uniaxial compaction in three stages: 35 MPa prior to insulation-and-curing, 10 MPa in preparation for reaction-heat treatment (RHT), and 10 MPa again prior to vacuum impregnation.

Also as described elsewhere [9] calorimetric and magnetic AC loss measurements were made at 4.2 K by boil-off calorimetery using facilities of the Low Temperature Division, Faculty of Applied Physics, University of Twente. The total AC loss per cycle, $Q_t(f) = Q_h + Q_{coup}(f)$, where Q_h is the strand's "persistent current" magnetization loss and $Q_{coup}(f)$ is the interstrand coupling loss, was generated by transverse AC fields of amplitude $B_m = 400$ mT and frequencies, f, of up to 90 mHz applied both "edge-on" (EO) and "face-on"

TABLE 1. The Strand and General Cable Details

The Strand			
Type	OST-RRP Billet No. 8879		
Diameter, mm	0.702		
Filament count	54(61)		
Estimated fill-factor, λ	0.5		
Filament diameter, d, μm	77		
The Cables			
General cable type	LBNL-wound LARP-TQ		
Strand count, N	27		
Transposition pitch, $2L_p$, mm	79.3		
CSMM code	1	2	1A
LBNL code	953R	954R	954A
Core width, mm	0	8.00	8.00
Condition*	A+R	A+R	A
Thickness, t, mm	1.26	1.26	1.31
Initial width, mm	10.06	10.06	10.03
Final width, w, mm**	10.15	10.25	10.12

* A = annealed 4h/200°C in flowing Ar; R = re-rolled
** The cable width increased during pack assembly in response to compactions prior to final heat treatment

(FO) to the cable . For comparison with the in-cable measurements, hysteretic loss, Q_h, and the associated persistent current magnetization, M_h, were measured on pieces of strand removed from the ends of the heat treated cable packs. These measurements were made at CSMM also to ± 400 mT by vibrating sample magnetometry (VSM) using a Quantum Design Model 6000 "physical property measuring system" (PPMS). The strand details are listed in TABLE 1.

Coupling Loss and Interstrand Contact Resistance

If the ICR is relatively large the AC loss is linear over the frequency range of the experiment such that $R_{\perp,eff}$ can be obtained from the reciprocal slope of Q_t vs f. But if ICR is small the full frequency dependence of f must be invoked. The simultaneous generation and decay of coupling currents gives rise to a maximum in $Q_t(f)$ at a critical

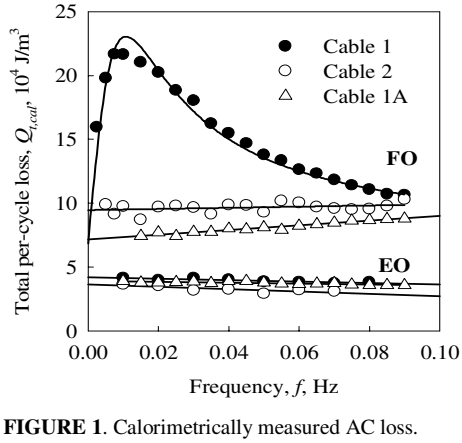

FIGURE 1. Calorimetrically measured AC loss.

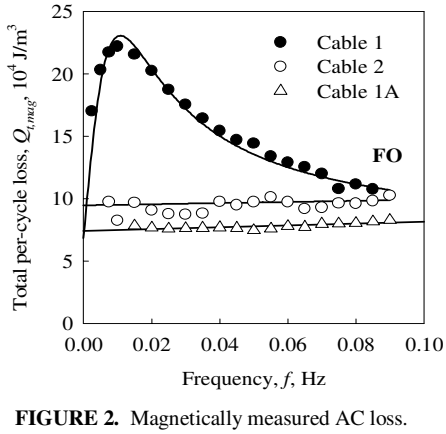

FIGURE 2. Magnetically measured AC loss.

TABLE 2. List of the Calorimetrically- and Magnetically Measured ICRs

CSMM Cable No.	Cable Type	Measurement Type	$R_{\perp eff}$, μΩ (init. Slope[a])	$R_{\perp eff}$, μΩ (init. fit[b])	f_c mHz	$R_{\perp eff}$ μΩ (from f_c)	$\langle R_{\perp eff} \rangle_{AV.}$ μΩ
1	No-core A+R	calorimetric	0.34	0.41	10.8	0.20	
1	"	magnetic	0.34	0.40	9.81	0.18	
Average	**No-core**						**0.31**
1A	Core A	calorimetric	64	--	--	--	
1A	"	magnetic	164	--	--	--	
Average	"						**114**
2	Core A+R	calorimetric	246	--	--	--	
2	"	magnetic	172	--	--	--	
Average	"						**209**
Average	**both core cables**						**162±75**

a) From the initial raw $Q_t(f)$ data (Cables 1) and the entire linear set (Cables 1A and 2)
b) From the fitted initial slope ($f \to 0$) of $Q_t(f) = Q_h + Q_0(f/f_c)[1+(f/f_c)^2]$, i.e. Q_0/f_c

frequency $f_c = 1/2\pi\tau_c$ (where τ_c is the corresponding relaxation time) following a general relationship $Q(f) = Q_0(f/f_c)/(1 - (f/f_c)^2)$ which applies both to strand eddy currents as well as cable- and cable-stack coupling currents. Relationships between the individual-cable relaxation time, τ_{cab}, and the relaxation time of the cable stack, τ_{stack}, lead to f_c-based ICR values herein designated $R_{\perp,fc}$. According to Verweij [3] $R_\perp = 2\pi(\mathrm{DE})f_c$, which is obtained by combining τ_{cab} $R_\perp$ = D (a function of the individual-cable properties N and L_p) with $\tau_{stack}/\tau_{cab} \equiv 1/(2\pi f_c \tau_{cab})$ = E (a function of (w/t) and the number of cables in the stack). Use is also made of the low-f limit of $Q(f)$ to obtain values of $R_\perp$ from the "raw" initial slope of $Q_\perp(f)$ (herein $R_{\perp,init\ slope}$) as well as from the fitted initial slope ($R_{\perp,init\ fit}$).

The results of the FO and EO calorimetric AC loss measurements and the FO magnetic measurements are shown in FIGURES 1 and 2 and summarized in TABLE 2. Note that the expected low ICR of the uncored cable, 0.3 μΩ, rises by more than a factor of 500 with the insertion of the full-width stainless steel core. During cable pack preparation the widths of Cables 1A and 2 (Table 1) increased by 0.09 mm and 0.19 mm, respectively. Given that for cored cables $R_{\perp,eff} = (N^3/20)R_{//} = 984R_{//}$ it seems that a possible loosening of the side-by-side contact allowed $R_{//}$ to increase from 0.12 μΩ to 0.21 μΩ.

Persistent-Current ("Hysteretic") Per-Cycle Loss and Magnetization

***Cable-Based Hysteretic Loss*:** The cable-based AC loss experiment is designed to measure coupling loss, ICR, and cable magnetization, the latter being a measure of dipole or quadrupole field error. The zero-f extrapolation of $Q(f)$ yields the persistent-current loss, Q_h. Since the strands are unpenetrated at the low B_m of the experiment (400 mT) the Q_h so obtained and its associated M_h have no particular relevance to magnet operation. However its relationship to individual-strand properties does provide some insight into the condition of the strand in the cable.

***Individual-Strand Hysteretic Loss*:** Magnetization loops for strand segments 1, 1A, and 2 taken using a field sweep amplitude, B_m, of 14 T are shown in FIGURE 3. In it we note that the fully penetrated strands exhibit partial flux jumping in fields less than 1 T. Also from the full height of the magnetization loop at 12 T the magnetic J_c at 4.2 K and that field can be obtained from $J_{c,mag} = \Delta M_h(3\pi/4)/(\lambda d)$ where λ is the strand fill factor and d the filament (subelement) diameter (TABLE 1). An average of 5 results for the three strand segments yielded ΔM_h = 47.1 ± 4.9 kA/m leading to $J_{c,mag} \cong 2900 \pm 300$ A/mm^2 either of which make useful starting points for estimating cable M_hs and J_cs at selected magnet operating points.

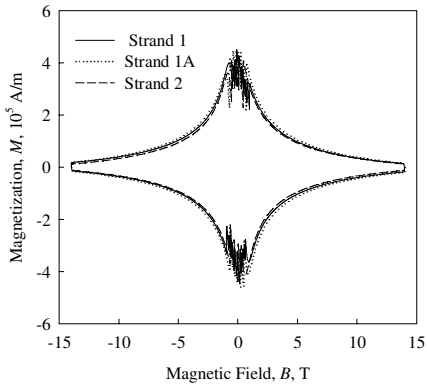

FIGURE 3. PPMS/VSM hysteresis loops at ±14 T

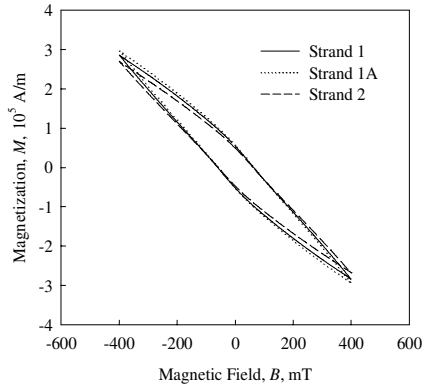

FIGURE 4. VSM hysteresis loops at ±400 mT

The unpenetrated magnetization loops are shown in FIGURE 4. The selection of the common field sweep amplitude of 400 mT enabled the in-cable- and extracted strand losses to be compared, as in TABLE 3. Note that the sweep rate selected for the magnetization measurements was 130 Oe/s which corresponds, according to the relationship $f = (dB/dt)/(4B_m)$, to a frequency of 8 mHz.

RESULTS

Interstrand Contact Resistance

During reaction-heat-treatment under uniaxial pressure the uncored cable develops very low crossover ICRs. For such cables the measured $R_{\perp eff}$ is essentially the actual crossover resistance, $R_{\perp}$. The value obtained, 0.31 μΩ, conforms well to the previous results of an extensive series of measurements (referred to in [9]) on uncored Nb_3Sn cables, $R_{\perp}$ values clustering around 0.28 ± 0.1 μΩ. To suppress the consequent interstrand coupling a core is needed to raise ICR into the 20 μΩ range, which for Cable 2 ramping at 6.5 mT/s corresponds to an $M_{h,4.2K}$ of 1.3 kA/m. The presently obtained $R_{\perp eff}$ = 162±75 μΩ, although it successfully reduces magnetization, is actually too large to secure stability. For this reason partial-width cores are recommended for Nb_3Sn cables, studies of which are now

TABLE 3. Hysteretic Losses of Cables and Extracted Strands

			AC Loss (Figures 2 and 3)			**Hysteresis Loops (Figure 5)**	
Name	Cable	Type	$FO_{cal.}$	$FO_{mag.}$	$EO_{cal.}$	Strand	0.9 x Strand[a]
1	No-core	A+R	-	-	**4.19**	4.61	**4.15**
1A	Core	A	7.15	7.41	**3.92**	4.72	**4.25**
2	Core	A+R	9.42	8.89	**3.62**	4.12	**3.71**

a) At a cable packing factor of 90% this normalizes the strand volume to the volume it occupies in the cable.

under way. Note that in the presence of insulated cross-over contacts our $R_{\perp eff}$ is to be taken, not as a resistance *per se*, but as a measure of interstrand coupling; it is of course $(N^3/20)R_{//}$. Data for Cables 1A and 2 (TABLE 1) show that re-rolling increases the cable width by 0.03 mm. However, any effect that this might have on ICR is masked by subsequent cable-preparation induced increases in width: 0.19 mm, Cable 2 (A+R) and 0.09 mm, Cable 1A (A only). The overall increase in cable width seems to lead to a reduction in the side-by-side contact and hence an increase in the measured $R_{\perp eff} \equiv (N^3/20)R_{//}$ shown in TABLE 2.

Magnetization of Fully Penetrated Strands, B_m = ± 14 T

From the *M(B)*-loop measurements, FIGURE 3, the persistent-current magnetization at 12 T is $M_h = \Delta M_h/2$ = 23.6 kA/m. That of the corresponding current-carrying cable at 4.2 K would be expected to be about $0.9(1-i^2)$, or 8.5 kA/m at i = 0.8. This is more than 6 times greater than the coupling magnetization indicating that, depending on the operating range of the magnet, consideration may need to be given to some form of magnetic compensation.

Magnetization of Partially Penetrated Strands, B_m = ± 400 mT

The edge-on cable loss, $Q_h = 3.9 \pm 0.3 \times 10^4$ J/m^3 can be accounted for in terms of the individual strand loss whose "cable-adjusted" value is $4.0 \pm 0.3 \times 10^4$ J/m^3. But in the FO orientation the cables exhibit enhanced magnetization losses such that $\langle Q_{h,FO} \rangle_{AV}/Q_{h,adj.strand}$ = 1.71 and 2.47 for Cables 1A and 2, respectively. It is hard to justify this in terms of individual strand deformation – flattening in the plane of the cable given that unpenetrated hysteretic loss is *inversely proportional* to strand diameter, d, and J_c. Hence the experimental results of Ghosh et al [10] on the fully penetrated magnetizations (directly proportional to $J_c \cdot d$) of rolled and reacted Nb_3Sn strands have no direct application to this case.

Microscopy has shown that the present strands and their outer subelements have undergone slight flattening during cabling and cable-pack preparation. However, in Strand 2 the observed strain ($\varepsilon = 1-\sqrt{r}$, where r is the aspect ratio [10]) being less than 8% would in any case have a negligible effect on the magnetization anisotropy. Furthermore, the persistent-current losses of Strand 2 measured in the FO and EO orientations to ±400 mT were the same within experimental error. However, FEM simulations, not presented here, suggest that the excess FO hysteretic loss may be tied to a demagnetization effect.

Strand and Cable Properties

We conclude by noting (i) the specific EO cable losses are the same as those of the individual extracted strands, (ii) based on a special experiment not described here, there is no discernable difference between the EO and FO losses of the slightly flattened extracted strands, (iii) the FO cable losses are typically twice as large as the EO values, (iv) although re-rolling increases the FO Q_h of Cable 2 it has no significant effect on that of the extracted strand, (v) the enhanced persistent-current loss of the cable may be due to a demagnetization effect. As such it would not be relevant for high field conditions, but could possibly be an effect near injection, depending on the specific values chosen.

CONCLUSION

Calorimetric and magnetic measurements of AC loss in Nb_3Sn Rutherford cables were used to extract values of ICR for one uncored cable and two cored cables. The uncored cable had an ICR of 0.3 μΩ, while for the cored cables the ICR was 114 μΩ (annealed) and 209 μΩ (annealed and re-rolled). Hysteretic loss intercepts for cable measurements with the field edge-on to the cable agreed with short sample PPMS measurements of strand hysteretic loss. On the other hand face-on hysteretic intercepts were high, possibly due to demagnetization effects. Lastly, while the need to reduce d_{eff} in Nb_3Sn strands for magnet field quality is well known, this present work gives an interesting result. Specifically, for

the present cored cables, the magnetization from persistent currents is six times greater than the coupling current magnetization at 14 T, and of course this ratio grows as the field drops. This result reinforces the need to reduce the d_{eff} in strands in order to improve field quality in accelerator magnets.

ACKNOWLEDGEMENTS

The cables were wound at LBNL by H.V. Higley. Initial compaction and heat treatment of the CSMM-mounted cable packs were performed at FNAL courtesy of E. Barzi, with the assistance of B. Bianchi. Further compaction prior to impregnation was performed at OSU by L. Barnhart and R. Baldwin. J. Yue, Hyper Tech Research Ltd, performed the vacuum impregnation with CTD-101 resin and curing of the cable packs. Scanning electron microscopy and related measurements were performed on cable segments by X. Peng, Hyper Tech Research Ltd. The U.S. Department of Energy, Office of High Energy Physics, funded the research at LBNL, FNAL, and CSMM, in the latter case under DE-FG02-95ER40900.

REFERENCES

1. M. Di Castro, L. Bottura, D. Richter, S. Sanfilippo, and R. Wolf, "Coupling current and AC loss in LHC superconducting quadrupoles", *IEEE Trans. Appl. Supercond.* **18** 108-111 (2008).
2. A. Devred, L. Bacquart, P. Bredy, C.E. Bruzek, Y. Laumond, et al., "Interstrand resistance measurements on Nb_3Sn Rutherford-type cables", *IEEE Trans. Appl. Supercond.* **9** 722-726 (1999).
3. A.P Verweij, "Electrodynamics of Superconducting cables in accelerator magnets" *Ph.D. Thesis*, University of Twente Press, 1995.
4. A.V. Zlobin, J.A. Johnstone, V.V. Kashikhin, N.V. Mokhov, I.L. Rakhno, et al., "Nb_3Sn quadrupols in the LHC Phase I upgrade", Proc. EPAC08 (Paper WEPD037, pp. 2491-2493), Genoa, Italy, 2008.
5. M.D. Sumption, R.M. Scanlan, Yu.A. Ilyin, A. Nijhuis, and E.W. Collings, "Magnetic, calorimetric, and transport studies of coupling and interstrand contact resistance in Nb_3Sn Rutherford cables with bimetallic cores of stainless steel bonded to copper", *Adv. Cryo. Eng. (Materials)* **50** 781-788 (2004).
6. E.W. Collings and M.D. Sumption, "Interstrand coupling and magnetization in Nb_3Sn Rutherford cables", *Proc. WAMSDO Workshop*, CERN, Geneva, Switzerland, 19-13 May (2008), pp. 42-50 -- available at http://care-hhh.web.cern.ch/CARE-HHH/LUMI-06/Proceedings/proceedings_lumi06.htm
7. M.D. Sumption, E.W. Collings, R.M. Scanlan, A. Nijhuis, and H.H.J. ten Kate, "Core-suppressed AC loss and strand-moderated contact resistance in a Nb_3Sn Rutherford cable", *Cryogenics* **39** 1-12 (1999).
8. L. Bottura, M. Buzio, S. Fartoukh, S. Russenschuck, S. Sanfilippo, W. Scandale, et al., "Field quality of the LHC dipole magnets in operating conditions", *LHC Project Report 573:* Proc. Eighth European PAC, June 2002, Paris, France.
9. E.W. Collings, M.D. Sumption, M.A. Susner, D.R. Dietderich, Y. Ilyin, and A. Nijhuis," Influence of a stainless steel core on coupling loss, interstrand contact resistance, and magnetization of an Nb_3Sn Rutherford cable", *IEEE Trans. Appl. Supercond.* **18** 1301-1304 (2008).
10. A.K. Ghosh, L.D. Cooley, D.R. Dietderich, and L. Sun, "Transport and magnetization properties of rolled RRP Nb_3Sn strands", *IEEE Trans. Appl. Supercond.* **18** 993-996 (2008).